Polymer 242 (2022) 124577

Contents lists available at ScienceDirect

Polymer

journal homepage: www.elsevier.com/locate/polymer

Effect of atomistic fingerprints on thermomechanical properties of epoxy-diamine thermoset shape memory polymers

Anwar Shafe [a], Collin D. Wick [a,*], Andrew J. Peters [a], Xiyuan Liu [a], Guoqiang Li [b]

[a] College of Engineering & Science, Louisiana Tech University, Ruston, LA, 71270, USA
[b] Mechanical & Industrial Engineering Dept, Louisiana State University, Baton Rouge, LA, 70803, USA

A B S T R A C T

Shape memory polymers (SMP) have been a field of interest for researchers over the past few decades and SMPs with unique characteristics are being developed continuously. Careful, time-consuming design is required for improved materials. Polymer informatics is part of an effort to shorten the development time of polymers by using computation and data-driven approaches such as machine learning. A specific polymer can be described via "fingerprints", which are a way to characterize molecular structures in a manner understandable by computers. In this paper, we describe combinations of nine epoxies and twenty-two hardeners with twenty fingerprints, and simulated the thermomechanical cycle with molecular dynamics code LAMMPS. Subsequently, we statistically analyzed which fingerprints are most strongly correlated with each shape memory property, specifically recovery stress and shape recovery ratio. This study lays a solid foundation for choosing and understanding atomistic fingerprints in order to discover new SMPs via machine learning.

1. Introduction

Shape Memory Polymers (SMP) are a type of material with the ability to change its shape in response to an external stimulus or trigger [1]. SMPs usually have one 'memorized' or permanent shape, which can then be deformed or 'programmed' to make another shape that can be held until a certain stimulus is applied. These stimuli can be heat [2–4], light [5], and other types of triggers [6,7]. When this occurs, the programmed shape returns to its original shape, often having a significant stress release that can be used for useful work, if partially constrained shape recovery is allowed. For example, a new kind of suture was developed using SMPs that automatically fastens itself using the body heat as trigger [8]. Smart curtains that can draw itself by reacting to sunlight has also been developed using SMPs [9]. Most heat-triggered SMP have one switch temperature above which it returns to its permanent shape [10]. In absence of thermal stimulus, other methods like magnetic, electrical and chemical stimuli have also been used to achieve remote actuation [11], for example, making implants on neural interfaces to understand neurological disorder [12], and developing shape memory hydrogels for drug delivery [13].

To better understand and address problems in polymer physics, theoretical, experimental and computational methods are used. Due to rapid advances in computation technology in recent years, modeling and studying polymers by computational methods is a way to shorten material development time. One standard tool for modeling polymers is molecular dynamics (MD) simulations [14]. MD can predict bulk properties of a variety of materials and elucidate the molecular level factors that contribute to these properties [15]. Large-scale data acquisition and analysis is also aided with MD with extensive use of automation. MD has been used to study variety of SMPs [16–23] utilizing both coarse-grained and atomistic models [17–19]. It has been used to quantify how different functional groups affect the shape memory behavior of a specific SMP. To better understand how different structural characteristics affect the shape memory property and deformation mechanism of SMPs, shape-memory polymers were modeled by simulating three epoxies and twenty-two curing agents using MD [20,21]. A coarse-grained model was also used to study the structure-property relationships of SMPs [22]. Some studies aimed to enhance the shape memory effect by modeling SMPs mixed with other materials such as graphene sheets [23].

As not all polymers exhibit a sufficient shape memory effect (SME) for all applications, appropriate material and structural design are required. The factors affecting the shape-memory properties (i.e., shape recovery ratio and recovery stress) need to be identified and manipulated. Polymer informatics is a new field of materials science being used to address such issues. It is a data-driven approach adopted because of the often complex nature of problems faced during new material discovery [24]. The power of any data-driven approach depends on the accuracy and how well the data is organized, and should be reproducible and accessible to others [25]. For this reason, The US Government

* Corresponding author.
E-mail address: cwick@latech.edu (C.D. Wick).

https://doi.org/10.1016/j.polymer.2022.124577
Received 18 October 2021; Received in revised form 12 January 2022; Accepted 20 January 2022
Available online 23 January 2022

launched a federal multi-agency initiative named 'Materials Genome Initiative' [26] in 2009 to discover and manufacture new materials within a fraction of the time of traditional methods as well as making collaboration easier. The UK, Germany, Spain, Italy [27], and Japan [28] have also established such databases.

The Polymer Genome Initiative was recently developed [29] for the rapid structure to property predictions of polymers with a single backbone and of ladder polymers. In order to translate molecular structures into a computationally meaningful representation, a new technique called "fingerprinting" was developed. It involves breaking down a molecule into a sequence of numerical values that define the chemical and physical properties of the molecule [30]. Examples of these descriptors include degree of branching, weight averaged molecular weight, polydispersity, chemical composition, electronegativity, HOMO-LUMO gaps, and radial distribution functions [31]. The fingerprints can be described in different length scales ranging from atomistic-scale, such as elemental composition, to topological scale, such as distance between rings, and to morphological descriptors, such as volume fraction of phases. A methodology to predict polymer properties using a dataset with descriptors and their associated properties was developed in a 2017 study [32]. An online platform named NanoMine, created to help design and predict the properties of new polymer nanocomposites, was also created [33]. Recently, 2000 unique coarse-grained polymers were simulated to create a dataset for reliably predicting structural properties with limited structural information [34]. Most recently, machine learning (ML) was used to discover new thermoset shape memory polymers (TSMPs) with a small training dataset [35]. In that study, the recently developed BigSMILES [36] was used to fingerprint the thermoset network. While BigSMILES is a useful tool, able to represent the sequency of the atoms within the monomer, crosslinker, and of the crosslink point, it does not directly include information about the topology, the interaction potential, or any higher order information about the structure. By including such information in the form of the fingerprints discussed here, the correlation between the chemical structures and thermomechanical properties of the TSMPs can be better established and understood, and more accurate predictions can be produced. Unfortunately, there are many ways to describe features within the monomers and hardeners, and it is not clear which features, or fingerprints, can strongly correlate with the thermomechanical properties, particularly the shape recovery ratio and recovery stress.

The goal of this study is to apply this approach to amine hardened epoxies. Specifically, the MD package LAMMPS [35] was used to simulate combinations of 9 epoxies, all with exactly two glycidyl ether groups (DGE), and 22 commercially available hardeners, each with two primary amine groups. Twenty descriptors or fingerprints, such as sidechain length, were chosen to represent the epoxies and hardeners. After crosslinking and relaxation, the fingerprints, defined in section III, were calculated. The glass transition temperature, recovery stress, and shape recovery ratio were then calculated, which are properties associated with SME. The effect of the fingerprints on their respective desired properties were calculated by analyzing their p-values and correlation coefficients.

2. Simulation details

II.A. Creation of Polymer Networks. We developed a set of Python codes to create polymer networks based on DGE epoxies and hardeners with two amine groups. The codes were designed to work with epoxies with DGE end groups and any amine hardener, requiring its SMILES (Simplified molecular-input line-entry system) string as input. The LigParGen software [36], which incorporates the SMILES of different molecules as inputs, was used to create the topology files for the monomers. These topologies were utilized as data files for the LAMMPS simulations software package [35,37] with the optimized potential for liquid simulations force field [38–40]. Also, using the LigParGen software, the topologies of reacted epoxies plus hardeners were saved to create the crosslinks in the polymer network. This is described in greater detail in our previous work [16].

We chose epoxies and hardeners so that each epoxy had exactly two glycidyl ethers, each hardener had two amine nitrogens, and each nitrogen had two hydrogens. This was done to be consistent with our previous work with DGEBA-IPD [16], which was calibrated against experiment for its crosslinking percentage, in which 70% was used. For the number of DGEs and amine hydrogens to be the same, the system configurations were constrained to have two epoxies for every hardener. A simulation box was created for every system with two epoxies and one hardener in which their individual structures were relaxed with conjugate gradient energy minimizations. Then, the systems were replicated six times in X, Y, and Z directions to create a total of 432 epoxies and 216 hardeners. This resulted in system sizes ranging from 18,240 to 30,240 atoms with 864 glycidyl ethers and amine hydrogens for a total of 864 potential reactions.

Table 1 gives a list of all epoxies and hardeners studied, including their abbreviations. Full chemical structures for each epoxy and hardener can be found in Tables S1 and S2. The specific procedure for equilibrating the systems, creating five independent structures, and carrying out the crosslinking is described in detail in our previous work [16]. We crosslinked all of the systems to create 70% of all possible bonds, which gave the best agreement with experimental glass transition values, rubbery and glassy moduli for DGE-IPD [16]. This resulted in approximately 90% of epoxy and nearly 100% of hardener monomers reacting at least once. Crosslinking was simulated at 398 K for all systems, with 10 ps of equilibration in 0.5 fs time steps preceding each crosslinking attempt at 1 atm in the NpT ensemble [41]. This was followed by bond rearrangement, and then a two-step relaxation procedure as detailed in our previous work [16], which was adopted from other works [42,43]. The process was repeated until 600 total steps were carried out. Each step resulted in a reaction between glycidyl ether and

Table 1
List of epoxies and hardeners modeled and their abbreviations.

Epoxy/Hardener	Abbreviation
Epoxies	
Bisphenol A DGE	DGEBA
Bisphenol F DGE	EPON862
Propoxylated bisphenol A DGE	DGEBAPO-2
Resorcinol DGE	DGER
Poly (ethylene glycol) DGE	DGEPEG
1,2-cyclohexanediol DGE	DGECD
1,7-dihydroxyl naphthalene DGE	DGEDHN
Neopentyl glycol DGE	DGENG
Poly (dimethylsiloxane) DGE	PDMSDGE
Hardeners	
Isophoronediamine	IPD
1,3-Bis(aminomethyl)cyclohexane	BACH
m-Phenylenediamine	MPDA
Propylenediamine	DAP
2,2-Bis(aminoethoxy)propane	BAP
2,4-Diaminotoluene	DAT
2,2′-(Ethylenedioxy)bis (ethylamine)	EDBE
Jeffamine	JA
m-Xylenediamine	XDA
4,7,10-Trioxa-1,13-tridecanediamine	TTD
Butylenediamine	DAB
Ethylenediamine	DAE
p-Phenylenediamine	PPDA
2,4-diethyl-6-methylbenzene-1,3-diamine	DMDA
Acetoguanamine	AGA
4-ethyoxybenzene-1,2-diamine	EOBA
4-phenylpyridine-2,6-diamine	PPYA
o-Phenylenediamine	OPDA
1,1′-Binaphthyl-2,2′-diamine	BPDA
Dytek EP Diamine	DEPD
3,4-Pyridinediamine	PDA
2,2′-Dithiodianiline	DOA

amine hydrogen, resulting in 69.4% of possible reaction pairs (600/864) forming bonds.

2.1. II.B. Calculation of shape memory properties

The glass transition (T_g) and other shape memory properties for each system were calculated in the same fashion as our previous work [16]. The uncertainties were calculated by the standard error of the mean from the five independent simulations. All systems were equilibrated at 30 K above their T_g values at a pressure of 1 atm to allow for hot programming, or deformation in their rubbery states, as was done by Fan and Li [44]. Programming was carried out by slowly applying a 50% compression in one direction while keeping the pressure perpendicular to the deformation set to 1 atm for 4 ns. For each of the five systems, three independent compressions were carried out, one for each dimension, leading to a total of 15 separate simulations. After programming, the systems were allowed to relax at a fixed strain in one direction for an additional 4 ns, followed by a 2 ns simulation in which the systems were cooled to 298 K at the same strain conditions. Then, a 2 ns simulation at 298 K was carried out in the NpT ensemble allowing all system directions to change, and allowing for a small elastic spring-back to occur. Next, the direction that had the initial deformation was fixed, allowing directions perpendicular to this equilibrate at 1 atm, and a 2 ns simulation warming the system to 30 K above their T_g took place, followed by an additional 2 ns simulation at 30 K higher than the T_g, which was used to calculate the recovery stress. This recovery stress was the stress along the same axis as deformation during the last 200 ps of the simulation.

An additional 4 ns simulation in the NpT ensemble was also carried out at 550 K and 1 atm, where all directions were allowed to have volume fluctuations to estimate the shape recovery. The shape recovery ratio was recorded at the end of the simulation period in the usual way [45]. The fixed temperature of 550 K was chosen for two reasons. A higher temperature allowed the system to equilibrate faster, allowing differences between the systems to be compared with relatively shorter simulations. Also, using the same temperature for all systems studied versus studying shape recovery at 30 K higher than their T_g allowed a better comparison between them. Our previous work found that using temperatures based on each system's individual T_g made it challenging to compare them as higher temperatures always lead to higher shape recovery in the short simulation times that we can run [16]. In reality, these higher temperatures may lead to additional side reactions that could further change the cross-linking ratio. However, in the simulations, this can be controlled, and the higher temperature is used for the sole purpose of increasing the dynamics of the system for the purpose of making a more consistent qualitative comparisons in their shape recovery ratios.

3. Fingerprinting

Fingerprinting for each polymer focused on the individual monomers before they were crosslinked. The first step in fingerprinting was defining which atoms are part of the backbone, and which are part of sidechains. Fig. 1 is a schematic for the heavy atoms for DGEBA and IPD, which shows all backbone atoms as black and sidechain atoms as red. For DGEBA, crosslinked networks are formed by reactions with the primary carbons in the epoxy groups, with the bonds between the primary epoxy carbons and the epoxy oxygens breaking during network formation. As a consequence, the epoxy oxygen atoms are treated as sidechain atoms. For both of these monomers, it can be observed that all atoms that form bonds between the reactive groups are classified as the backbone.

The following fingerprints were used to describe the individual monomers.

1) The number of bonds separating the shortest distance between the reacted DGE carbons. In the case of DGEBA (see Fig. 1), this is 16.
2) The number of bonds separating the shortest distance of reacted amine nitrogens. For IPD, this is 5.
3) The average number of backbone heavy atoms after full crosslinking divided by the number of original monomers. Note that in a ring, this will include all ring atoms. This is $(2 \times 21 + 9)/3 = 17$ for DGEBA-IPD (note that DGEBA has twice as many monomers as IPD).
4) The ratio of the number of backbone heavy atoms with the total number of heavy atoms. For instance, in DGEBA, there are 21 backbone atoms and in IPD there are 9 (see Fig. 1). That gives a total of 51 backbone atoms since there are two DGEBA for every IPD. The total number of heavy atoms for DGEBA and IPD are 25 and 12, respectively, giving a total of 61 heavy atoms. This gives a ratio of $51/62 = 0.823$.
5) The stiffness of the bond stretching interaction between heavy atoms. Bond stretching is given by the following formula: $u_{bond} = k_r(r - r_0)^2$. The stiffness is simply the average k_r for all bonds.
6) The stiffness of the angular interaction between heavy atoms (see Fig. 1). Angles interact via the harmonic formula: $u_{angle} = k_\theta(\theta - \theta_0)^2$. The stiffness is the average k_θ for all angles.
7) Dihedral energy strength between heavy atoms (see Fig. 1). Dihedrals interact via both regular dihedral energy and improper torsional energy:

$$u_{dihedral} = \frac{1}{2}k_1[1 + \cos(\varphi)] + \frac{1}{2}k_1[1 + \cos(2\varphi)] + \frac{1}{2}k_1[1 + \cos(3\varphi)] + \frac{1}{2}k_1[1 + \cos(4\varphi)] + K[1 + d\cos(n\varphi)] \quad (1)$$

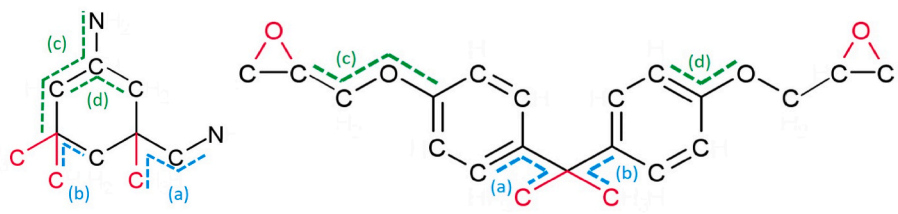

Fig. 1. Schematic for the fingerprinting scheme for IPD (left) and DGEBA (right). Black bonds and atoms are part of the backbone, while those marked red are part of the sidechain. Light blue dashed lines indicate sidechain bond angles and sidechain dihedrals; green dashed lines indicate backbone bond angles and dihedrals. Here, (a) and (b) are sidechain dihedral and bond angles, (c) and (d) are backbone dihedral and bond angles. (For interpretation of the references to colour in this figure legend, the reader is referred to the Web version of this article.)

The dihedral energy strength is defined as the sum of all $\left|\frac{k}{2}\right|$ values and $|K|$. Since these are sometimes negative, the absolute value is used.

8) The van der Waals (vdW) size as defined as the average σ value of the heavy atom Lennard-Jones potential which is used for vdW interactions:

$$u_{\mathrm{vdW}} = 4\varepsilon\left[\left(\frac{\sigma}{r}\right)^{12} - \left(\frac{\sigma}{r}\right)^{6}\right] \tag{2}$$

9) The van der Waals strength as defined as the average ε value of the heavy atom Lennard-Jones potential which is used for vdW interactions (Equation (2)).
10) The polarity of all the atoms. This is defined as the average electron charge squared (q_i^2) per atom.
11) The radius of gyration for the epoxy monomer and the hardener monomer. This is calculated based on the mass (with r_{COM} being the center of mass) [46],

$$R_g = \sqrt{\frac{\sum_{i=1}^{N} m_i \left(\vec{r}_i - \vec{r}_{\mathrm{COM}}\right)^2}{\sum_{i=1}^{N} m_i}} \tag{3}$$

12) The maximum sidechain length for heavy atoms. For an individual sidechain heavy atom, its sidechain length is defined as the number of bonds between it and the nearest backbone atom.
13) The number of aromatic and non-aromatic backbone rings. It should be noted that there are two epoxies for each hardener, so each epoxy is counted twice in this. For instance, DGEBA in a network will contribute four aromatic rings.

For items 5–10, fingerprints were calculated for both backbone and non-backbone or sidechain atoms. A bond, angle, or dihedral are considered part of the backbone only if *all* of the atoms are part of the backbone (see Fig. 1 for examples).

4. Results and discussion

4.1. IV.A. Calculated properties

Fig. 2 (left) illustrates the programming stress as a function of strain for four of the systems studied with 70% crosslinking: DGEBA epoxy with IPD, BACH, DAP, and PDA hardeners. All four of the systems have similar programming stress curves, and it would be expected that all of them would overpredict the stress in comparison with experiment due to the short simulation times (4 ns). Of greater interest is the recovery stress, which is also shown in the figure using triangle markers. In comparison with the programming stress, the recovery stress is much lower, consistent with experimental work [44]. The final recovery stress is also expected to be overpredicted due to the short simulation times (by around a factor of three in our previous work [44]), but the qualitative differences should be consistent. For instance, DGEBA-IPD has a higher recovery stress than DGEBA-BACH, which are the only two systems compared experimentally [44]. This is consistent with the results shown here despite the fact that the programming stress are nearly identical between the two systems. We are currently working on coarse-graining simulations to better bridge the timescale gap between simulations and experiment.

The shape recovery ratio (see section II·B) as a function of time for the four systems described is shown in Fig. 2 (right). As described, the temperature for this calculation was 550 K to increase the rate of shape recovery and to use the same temperature for comparisons for all systems. After 1–2 ns, the rate of shape recovery appears to stabilize to a

Table 2
Recovery stress (σ_{rec}) and shape recovery ratio (R_r) after 3 ns calculated for selected TSMPs.

Epoxy	Hardener	σ_{rec} (MPa)	R_r
DGEBA	IPD	50	0.50
	BACH	44	0.58
	MPDA	56	0.49
	DAP	60	0.68
	BAP	28	0.51
	DAT	50	0.55
	EDBE	49	0.66
	JA	39	0.94
	XDA	43	0.54
	TTD	44	0.71
	DAB	52	0.59
	DAE	56	0.56
	PPDA	47	0.38
	DMDA	53	0.46
	AGA	50	0.33
	EOBA	44	0.40
	PPYA	56	0.36
	OPDA	60	0.47
	BPDA	28	0.35
	DEPD	57	0.40
	PDA	56	0.42
	DOA	47	0.33
EPON862	IPD	40	0.48
DGEBAPO-2		29	0.67
DGER		43	0.52
DGEPEG		28	0.68

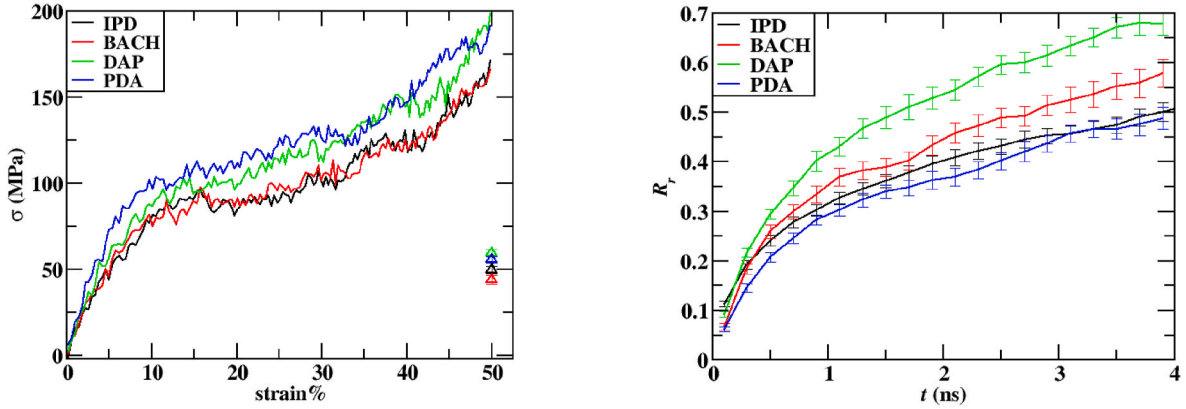

Fig. 2. Plot of recovery stress vs strain (left) and recovery ratio vs time (right). The recovery stress is shown in the left plot using triangle markers.

certain degree, increasing at a fairly constant rate.

Table 2 lists the recovery stress and shape recovery ratios calculated for a selected set of thermoset shape memory polymers (TSMPs) studied in this work, which include DGEBA with all hardeners studied and IPD with all epoxies. Table S3 includes a comprehensive list of all systems studied including their T_g values, which has more epoxy and hardener combinations than those shown in Table 2. The recovery stress is given at 30 K higher than T_g for all of them, consistent with our previous work [16]. As stated before, the crosslinking density is 70% for all of them, which was calibrated for DGEBA-IPD in our previous work [16]. The actual crosslinking density will most likely vary among the different systems, but a single one was chosen to make consistent comparisons between various TSMP networks. The first thing that can be observed is that out of all of the epoxies studied, DGEBA has the highest recovery stress. The two systems with literature experimental results, DGEBA-IPD and DGEBA-BACH, with similar programming and recovery criteria as the computational work, have experimental recovery stresses near 18 MPa and 9 MPa, respectively [44]. This shows that while the computationally predicted recovery stresses are higher than experimental value, the qualitative values, in this instance, are consistent. As indicated previously, the reason is due to our short simulation time. With longer simulation time, the recovery stress will be reduced due to stress relaxation, and the shape recovery ratio will increase due to structural relaxation, moving towards the experimental results.

A recovery stress temperatures 30 K higher than T_g was chosen to be consistent with previous simulation and experimental work [16, 44]. This results in most of the systems having their recovery stress being calculated at different temperatures for the TSMPs, which may have an impact on comparing them. To evaluate this, we calculated the recovery stresses of seven TSMPs at a set temperature of 210 °C, and the results are given in Table S3. For these seven TSMPs, the correlation coefficient between the recovery stress calculated at 30 K higher than T_g and those calculated at 210 °C is 0.997. This shows strong correlation between them, and it is expected that the correlation with the different fingerprints should only be minimally impacted by the fact that recovery stresses were calculated at different temperatures.

The shape recovery ratios after 4 ns vary widely among the different systems, ranging from 0.33 for DGEBA-DOA to 0.94 for DGEBA-JA. Upon closer inspection of these values, recovery stress values appear to be negatively correlated with R_r, which is consistent with previous observations. As indicated by Fan and Li [46], for a given polymer, lower stiffness in the rubbery state favors a higher shape recovery ratio, but reduces the recovery stress. This leads to a general assumption that recovery stress is negatively correlated with shape recovery ratio. To better demonstrate this, along with how the recovery stress and R_r correlate with glass transition temperature, Fig. 3 gives a comparison between scaled values with a linear regression line for their best fit. The recovery stress has a correlation coefficient (cc) of −0.27 and a p-value of 0.11 with R_r, while T_g has a 0.42 cc and 0.01 p-value with recovery stress and a −0.28 cc and a p-value of 0.10 with R_r. This shows that only the recovery stress and T_g have a statistically significant correlation (p-value less than 0.05). This consistent with a recent experimental study by Feng and Li [49], where they showed that a high glass transition temperature of 280 °C lead to a high recovery stress of 35.3 MPa in the rubbery state. While previous researchers have suggested that recovery stress and R_r were negatively correlated [46], and it could be difficult to increase both of these properties simultaneously, we find that the relationship is not universally true. The large scatter of values in the plot also is consistent with this, which shows that while there does appear to be a negative correlation between recovery stress and R_r, there are enough exceptions to allow a TSMP to be designed that has high values in both.

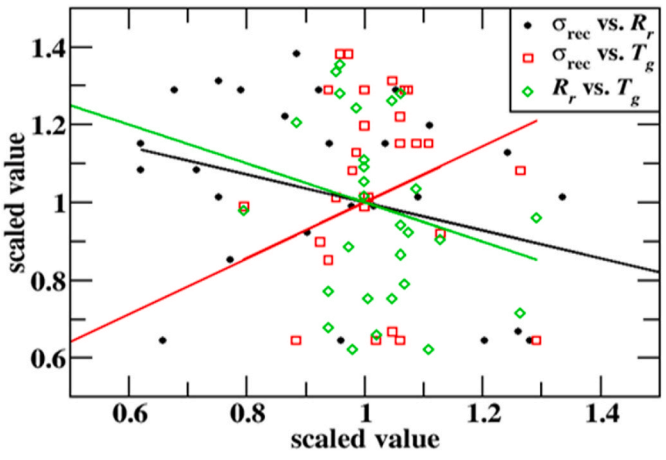

Fig. 3. Comparison of scaled recovery stress (σ_{rrec}), recovery ratio (R_r) and glass transition temperature (T_g) with respect to each other. The line represents the linear best fit between them. All values are scaled with respect to their mean.

4.2. IV.B. Correlation between fingerprints and properties

Table 3 gives some of the fingerprint values arrived at for a select number of epoxies, while Table S4 in the supplementary information gives a comprehensive list for all systems and values. BB and SC refer to the backbone and sidechain, respectively. Each epoxy and hardener combination requires approximately 1 min to calculate, as their minimum energy structures need to be generated with the LigParGen software [36]. One may notice that the radius of gyration, R_g, of the same epoxies vary to a modest degree. This is due to the fact that the minimum energy structures of the systems used to calculate R_g created by the LigParGen software [36] had a slight variation in structures, because it uses a Monte Carlo procedure for minimization. Many of the values themselves appear to make qualitative sense. For instance, the stretching energies are much higher than angular, which are higher than dihedral. The backbone ratio shows that for most systems, the vast majority of the heavy atoms are part of the backbone. Furthermore, the epoxies have a more extended shape than the hardeners. Another aspect that can be observed is that vdW strength (i.e. the epsilon value in Equation (2)) has a strong correlation with polarity. This is expected as more polar molecules often have stronger vdW attraction.

Fig. 4 plots the recovery stress versus some of the fingerprint values calculated with lines representing linear fits of the data. All of the fingerprints are scaled by dividing their individual values by their means. As can be observed, the bond stretching and angular stiffness values are positively correlated with higher recovery stress. The SC dihedral stiffness has no significant correlation with recovery stress, while the BB dihedral stiffness does. The BB polarity has a negative correlation with recovery stress, while the number of aromatic BB rings (Arom. BB Rings) has a positive correlation with recovery stress. The latter observation is consistent with the results for BB stiffness, as aromatic rings have a high degree stiffness.

A plot of the shape recovery ratio, R_r, with selected fingerprints is given in Fig. 5. All of the stiffness values are negatively correlated with R_r, opposite with what was found for recovery stress and consistent with the negative correlation between σ_{rec} and R_r found in Fig. 3. Also, this is consistent with previous findings that stiffer polymers in rubbery state leads to lower shape recovery ratio [46]. It should be noted that SC angular and dihedral stiffness has weaker correlations than BB stiffness, showing most of the impact of stiffness is in the BB. The polarity of the BB has no significant correlation with R_r despite that it correlates with higher recovery stress. This makes changing BB polarity a potential way to increase recovery stress without impacting shape recovery. The number of BB aromatic rings is also negatively correlated with R_r, which is not surprising as aromatic rings are very stiff.

The p-values and cc's for all fingerprints with respect to recovery stress and R_r are given in Table 5. Fingerprints whose p-values are less

Table 3
Fingerprints for select epoxy and hardener combinations. The rest are included in the supplementary information.

Epoxy	Hardener	Epoxy Length	Hardener Length	Stretch (SC)	Stretch (BB)	Angle (SC)	Angle (BB)	Polarity (SC)	Polarity (BB)
DGEBA	IPD	16	5	385	287	47.7	42.8	0.059	0.03
DGEBA	BACH	16	5	383	304	47.1	41.4	0.04	0.042
DGEBA	MPDA	16	4	415	315	48.7	41.8	0.044	0.05
EPON862	IPD	16	5	385	298	46.7	40.8	0.059	0.031
DGEBAPO2	IPD	22	5	370	282	46.8	42.2	0.056	0.027
DGER	IPD	10	5	366	298	46	40.8	0.08	0.034
DGEPEG	IPD	9	5	299	298	42.2	40.8	0.092	0.031
DGECD	IPD	9	5	291	298	42.9	40.8	0.080	0.027
DHEDHN	IPD	11	5	389	298	49	40.8	0.064	0.033
DGENG	IPD	10	5	297	287	43	42.3	0.086	0.028
PDMSDGE	IPD	19	5	309	261	42.4	40.8	0.567	0.066

		vdW Size (SC)	vdW Size (BB)	vdW Strength (SC)	vdW Strength (BB)	BB Ratio	Epoxy R_g	Hardener R_g
DGEBA	IPD	3.467	3.391	0.078	0.079	0.823	4.795	2.450
DGEBA	BACH	3.471	3.344	0.076	0.094	0.85	4.815	2.503
DGEBA	MPDA	3.476	3.344	0.077	0.094	0.845	5.051	1.956
EPON862	IPD	3.476	3.329	0.078	0.087	0.879	4.835	2.452
DGEBAPO2	IPD	3.435	3.420	0.081	0.076	0.808	6.519	2.452
DGER	IPD	3.438	3.329	0.082	0.087	0.841	3.748	2.450
DGEPEG	IPD	3.400	3.329	0.085	0.087	0.806	3.749	2.450
DGECD	IPD	3.422	3.329	0.081	0.087	0.841	3.001	2.450
DHEDHN	IPD	3.453	3.329	0.081	0.087	0.865	3.713	2.450
DGENG	IPD	3.406	3.391	0.083	0.079	0.738	3.042	2.452
PDMSDGE	IPD	3.429	3.437	0.090	0.074	0.721	4.318	2.450

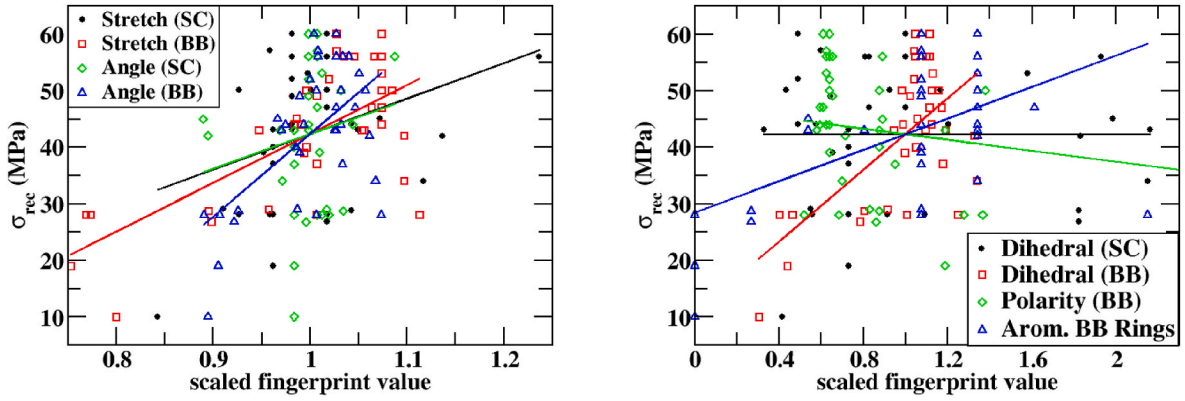

Fig. 4. Plot of the recovery stress with respect to selected fingerprint values. All fingerprints are scaled with respect to their mean values.

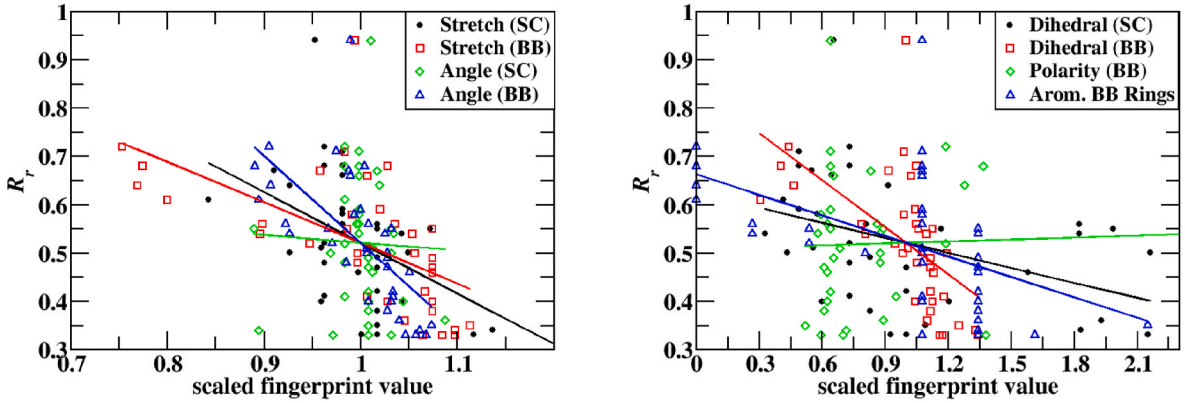

Fig. 5. Plot of the shape recovery ratio with respect to selected fingerprint values. All fingerprints are scaled with respect to their mean values.

Table 5
P-value and Pearson correlation coefficient for different fingerprints with recovery stress (σ_{rec}) and shape recovery ratio (R_r).

Fingerprint	σ_{rec} (MPa)		R_r	
	p-value	cc	p-value	cc
Epoxy Length	0.08	0.29	0.99	0.00
Hardener Length	0.45	−0.13	**< 0.01**	**0.51**
BB Ratio	**0.05**	**0.33**	0.19	−0.22
Stretch (SC)	**0.04**	**0.35**	**< 0.01**	**−0.52**
Stretch (BB)	**< 0.01**	**0.68**	**< 0.01**	**−0.59**
Angle (SC)	0.32	0.17	0.81	−0.04
Angle (BB)	**< 0.01**	**0.60**	**< 0.01**	**−0.66**
Dihedral (SC)	0.99	0.00	**0.01**	**−0.41**
Dihedral (BB)	**< 0.01**	**0.63**	**< 0.01**	**−0.58**
vdW size (SC)	0.67	−0.07	0.17	0.23
vdW size (BB)	**< 0.01**	**0.65**	**< 0.01**	**−0.57**
vdW strength (SC)	0.12	0.26	0.07	−0.30
vdW strength (BB)	**< 0.01**	**−0.58**	0.36	0.16
Polarity (SC)	0.52	0.11	0.03	−0.36
Polarity (BB)	**< 0.01**	**−0.51**	0.44	0.13
Epoxy R_g	**0.02**	**0.40**	0.86	−0.03
Hardener R_g	0.24	−0.20	**0.01**	**0.41**
Max SC Length	0.40	0.15	0.12	−0.26
Non-Arom. BB Rings	**< 0.01**	**−0.49**	0.12	0.26
Arom. BB Rings	**< 0.01**	**0.56**	**< 0.01**	**−0.51**

than 0.05 are considered statistically significant (i.e. having a confidence greater than 95%), and are shown in boldface. As described previously, all BB stiffness values (stretch, angle, and dihedral) are positively correlated with recovery stress and negatively correlated with R_r. Previous experimental work denoted the importance of enthalpy for having a high recovery stress [44]. While they focused on bond stretching energy, it appears that all types of bonding energy play a role in higher recovery stress with the notable exception of the backbone angular energy, which is also consistent with another theoretical study [50]. Unfortunately, these energies appear to negatively influence R_r as well. In addition, it is found that non-bonded interactions, in particular the polarity of the backbone atoms and their vdW strength lead to lower recovery stress. However, these two properties have no statistically significant impact on R_r. This shows from a design perspective that, polymers with stiff bonds but also with non-polar sidechains should be chosen for higher recovery stress. The fact that backbone atomic polarity and vdW strength has no statistically significant impact on recovery stress is also notable. The number of aromatic backbone rings has the same correlation with recovery stress and R_r as backbone stiffness as mentioned previously. Non-aromatic backbone rings (Non-Arom. BB Rings) are negatively correlated with recovery stress while having little to no correlation with R_r. Beyond the strength of interactions, the size of backbone atoms (i.e. bulkier atoms) is negatively correlated with higher recovery stress, but is not correlated with R_r. Furthermore, having more of the atoms a part of the backbone is positively correlated with recovery stress, while having a negative correlation, while not statistically significant, with R_r.

Sidechain fingerprints, in general, have little correlation with either recovery stress and R_r. This includes maximum sidechain length, (Max SC Length), angular sidechain stiffness, sidechain vdW strength and size, and sidechain polarity. The bond stretching stiffness is an exception, along with the dihedral stiffness with regard to R_r, potentially allowing further handles for σ_{rec} and R_r to be independently manipulated. Somewhat surprising, longer maximum sidechain length has no statistically significant correlation with recovery stress or with R_r. However, this study was limited to relatively short side-chains – the longest was 4 heavy atoms – and side chains longer than the backbones may produce different effects.

For designing new TSMPs, a few fingerprints stand out as correlating with only one of the properties in a statistically significant way, which could potentially be used to create a TSMP with both high recovery stress and R_r. The hardener length, which is defined as the number of atoms in between the amine groups, is correlated with higher R_r, and having a higher ratio of heavy atoms being a part of the backbone is positively correlated with recovery stress with only weak correlation with R_r. Additionally, the radius of gyration of the epoxy is significantly correlated only with recovery stress, while for the hardener, it is only significantly correlated with R_r. This, along with the results for the epoxy and hardener lengths, suggest that the epoxy length and how extended its structure is (since a more extended structure has a higher radius of gyration) increases recovery stress, while for the hardener, these increase R_r. Most of the other fingerprints appear to counterbalance one another, correlating with an increase in one, and a decrease in the other.

5. Conclusions

In this study, combinations of epoxies and amine hardeners were simulated for their shape memory properties. Overall, 11 out of 20 (55%) fingerprints show statistical significance with the recovery stress, and 9 out of 20 (45%) fingerprints show statistical significance with the shape recovery ratio. Some of these are consistent with many previous understandings. For example, overall backbone stiffness is expected to positively correlate with recovery stress as found in this study. However, sidechain stiffness has a much weaker correlation with recovery stress, if any at all. It is possible that higher sidechain stiffness plays a role in better crosslinking and consequently influencing recovery stress. At the same time, some of the fingerprints only affected one of the shape memory parameters. The backbone polarity, for example, significantly affected stress recovery, but does not affect the recovery ratio, suggesting that the stress recovery could be increased without penalty to the recovery ratio by manipulating the polarity along the backbone. The van der Waals strength behaves similarly. Backbone ratio was also significantly correlated with stress recovery, but not recovery ratio, adding another handle by which to manipulate only 1 shape memory property. Interestingly, the epoxy radius of gyration was only significantly correlated with the recovery stress, while the hardener radius of gyration was only significantly correlated with the recovery ratio, suggesting that applying machine learning approaches to these materials and fingerprints would likely result in materials with multiple property improvements.

However, this study doesn't focus on the impact of how fingerprints influence the crosslinking rate, and more studies, along with additional experimental validation would be necessary for such an investigation. Other limitations include: (1) epoxies with groups other than diglycidyl ether and hardeners with more than two amine groups were not included, (2) the LigParGen software cannot create topologies for molecules containing more than 200 atoms, limiting the candidates for epoxies and hardeners, and (3) computational timescale limitations prevented full recovery simulation of the polymers, necessitating extrapolation from short-timescale runs. (4) The amount of experimental data on shape memory properties is very limited, only providing two systems to make direct comparisons with. Regardless, this study provides useful guidance in selecting atomistic and topological fingerprints to represent the chemical structures and monomers and hardeners in machine learning, i.e., not all the fingerprints are strongly correlated with the thermomechanical properties, and those with strong correlations should be chosen in machine learning studies. Furthermore, the systems predicted to have high recovery stress are being synthesized to bring further experimental verification of the computational results and determine if increased recovery stress can be achieved.

It should be noted that all of the epoxies and hardeners simulated in this study are commercially available. Some of the fingerprints have a strong correlation with recovery stress and shape recovery ratio. However, due to their p-value not meeting the criteria, this correlation is not considered statistically significant. Perhaps a more extensive dataset will grant us more insight into the effect individual fingerprints have on shape memory properties. In future works, epoxies and hardeners that are not commercially available should be simulated to prepare a larger

dataset and discover new SMPs with better shape memory properties. Moreover, there are some intercorrelations within these fingerprints, which may require dimensional reduction methods (e.g., Principal Component Regression and LASSO) to give more accurate data analysis for machine learning to give more accurate data analysis.

CRediT authorship contribution statement

Anwar Shafe: Writing, Formal analysis. **Collin D. Wick:** Conceptualization, Investigation, Methodology, Software, Writing, Supervision. **Andrew J. Peters:** Conceptualization, Methodology, Writing, Supervision. **Xiyuan Liu:** Formal analysis. **Guoqiang Li:** Conceptualization, Project administration.

Declaration of competing interest

The authors declare that they have no known competing financial interests or personal relationships that could have appeared to influence the work reported in this paper.

Acknowledgements

This work is supported by the US National Science Foundation under grant number OIA-1946231 and the Louisiana Board of Regents for the Louisiana Materials Design Alliance (LAMDA). The high-performance computing resources provided by the Louisiana Optical Network Infrastructure (https://loni.org) were used for this work.

Appendix A. Supplementary data

Supplementary data to this article can be found online at https://doi.org/10.1016/j.polymer.2022.124577.

References

[1] Y. Xia, Y. He, F. Zhang, Y. Liu, J. Leng, A review of shape memory polymers and composites: mechanisms, materials, and applications, Adv. Mater. 33 (2021) 1–33, https://doi.org/10.1002/adma.202000713.
[2] G.J. Berg, M.K. McBride, C. Wang, C.N. Bowman, New directions in the chemistry of shape memory polymers, Polymer 55 (2014) 5849–5872, https://doi.org/10.1016/j.polymer.2014.07.052.
[3] Q. Zhao, H.J. Qi, T. Xie, Recent progress in shape memory polymer: new behavior, enabling materials, and mechanistic understanding, Prog. Polym. Sci. (2015) 79–120, https://doi.org/10.1016/j.progpolymsci.2015.04.001, 49–50.
[4] M.D. Hager, S. Bode, C. Weber, U.S. Schubert, Shape memory polymers: past, present and future developments, Prog. Polym. Sci. (2015) 3–33, https://doi.org/10.1016/j.progpolymsci.2015.04.002, 49–50.
[5] K.M. Lee, H. Koerner, R.A. Vaia, T.J. Bunning, T.J. White, Light-activated shape memory of glassy, azobenzene liquid crystalline polymer networks, Soft Matter 7 (2011) 4318, https://doi.org/10.1039/c1sm00004g.
[6] M.Y. Razzaq, M. Behl, U. Nöchel, A. Lendlein, Magnetically controlled shape-memory effects of hybrid nanocomposites from oligo(ω-pentadecalactone) and covalently integrated magnetite nanoparticles, Polymer 55 (2014) 5953–5960, https://doi.org/10.1016/j.polymer.2014.07.025.
[7] Y. Liu, Y. Li, H. Chen, G. Yang, X. Zheng, S. Zhou, Water-induced shape-memory poly(d,l-lactide)/microcrystalline cellulose composites, Carbohydr. Polym. 104 (2014) 101–108, https://doi.org/10.1016/j.carbpol.2014.01.031.
[8] A. Lendlein, Biodegradable, elastic shape-memory polymers for potential biomedical applications, Science 296 (2002) 1673–1676, https://doi.org/10.1126/science.1066102.
[9] G.K. Stylios, T. Wan, Shape memory training for smart fabrics, Trans. Inst. Meas. Control 29 (2007) 321–336, https://doi.org/10.1177/0142331207069479.
[10] A. Lendlein, S. Kelch, Shape-Memory Effect from permanent shape, Angew Chem. Int. Ed. Engl. 41 (2002) 2034–2057.
[11] M.Y. Razzaq, M. Behl, A. Lendlein, Memory-effects of magnetic nanocomposites, Nanoscale 4 (20) (2012) 6181–6195, https://doi.org/10.1039/c2nr31332d.
[12] T. Ware, D. Simon, K. Hearon, C. Liu, S. Shah, J. Reeder, N. Khodaparast, M. P. Kilgard, D.J. Maitland, R.L. Rennaker, W.E. Voit, Three-dimensional flexible electronics enabled by shape memory polymer substrates for responsive neural interfaces, Macromol. Mater. Eng. 297 (2012) 1193–1202, https://doi.org/10.1002/mame.201200241.
[13] O. Pillai, R. Panchagnula, Polymers in drug delivery, Curr. Opin. Chem. Biol. 5 (2001) 447–451, https://doi.org/10.1016/S1367-5931(00)00227-1.
[14] J.H.R. Clarke, D. Brown, Molecular dynamics modelling of polymer materials, Mol. Simulat. 3 (1989) 27–47, https://doi.org/10.1080/08927028908034618.
[15] M.P. Allen, in: Computer Simulation of Liquids, Oxford University Press, 1987.
[16] C.D. Wick, A.J. Peters, G. Li, Quantifying the contributions of energy storage in a thermoset shape memory polymer with high stress recovery: a molecular dynamics study, Polymer 213 (2021), https://doi.org/10.1016/j.polymer.2020.123319 submitted for publication.
[17] J. Diani, K. Gall, Molecular dynamics simulations of the shape-memory behaviour of polyisoprene, Smart Mater. Struct. 16 (2007) 1575, https://doi.org/10.1088/0964-1726/16/5/011.
[18] B.C. Abberton, W.K. Liu, S. Keten, Coarse-grained simulation of molecular mechanisms of recovery in thermally activated shape-memory polymers, J. Mech. Phys. Solid. 61 (2013) 2625–2637, https://doi.org/10.1016/j.jmps.2013.08.003.
[19] J. Moon, J. Choi, M. Cho, Programmed shape-dependence of shape memory effect of oriented polystyrene: a molecular dynamics study, Polymer 102 (2016) 1–9, https://doi.org/10.1016/j.polymer.2016.08.096.
[20] H. Yang, K. Zou, X.Y. Liang, Investigation of thermomechanical behaviors of epoxy shape memory polymers by molecular dynamics simulation, Appl. Mech. Mater. 273 (2013) 463–467. https://doi.org/10.4028/www.scientific.net/AMM.273.463.
[21] H. Yang, Z.D. Wang, Y.F. Guo, X.H. Shi, A molecular dynamics investigation of the deformation mechanism and shape memory effect of epoxy shape memory polymers, Sci. China Phys. Mech. Astron. 59 (2016) 1–7, https://doi.org/10.1007/s11433-015-5758-4.
[22] J.D. Davidson, N.C. Goulbourne, Microscopic mechanisms of the shape memory effect in crosslinked polymers, Smart Mater. Struct. 24 (2015), https://doi.org/10.1088/0964-1726/24/5/055014.
[23] M. Amini, K. Hasheminejad, A. Montazeri, Experimentally guided MD simulation to enhance the shape memory behavior of polymer-based nanocomposites: towards elaborating the underlying mechanism, Composer Part A Appl. Sci. Manuf. 138 (2020) 106055, https://doi.org/10.1016/j.compositesa.2020.106055.
[24] D.J. Audus, J.J. De Pablo, Polymer informatics: opportunities and challenges, ACS Macro Lett. 6 (2017) 1078–1082, https://doi.org/10.1021/acsmacrolett.7b00228.
[25] L. Himanen, A. Geurts, A.S. Foster, P. Rinke, Data-driven materials science: status, challenges, and perspectives, Adv. Sci. 6 (2019) 1900808, https://doi.org/10.1002/advs.201900808.
[26] Materials genome initiative, n.d. https://www.mgi.gov.
[27] Novel materials discovery (NOMAD) lab (n.d.), https://nomad-lab.eu.
[28] Materials research by information integration (n.d.), https://www.nims.go.jp/MII-I/en/.
[29] C. Kim, A. Chandrasekaran, T.D. Huan, D. Das, R. Ramprasad, Polymer genome: a data-powered polymer informatics platform for property predictions, J. Phys. Chem. C 122 (2018) 17575–17585, https://doi.org/10.1021/acs.jpcc.8b02913.
[30] T. Le, V.C. Epa, F.R. Burden, D.A. Winkler, Quantitative structure-property relationship modeling of diverse materials properties, Chem. Rev. 112 (2012) 2889–2919, https://doi.org/10.1021/cr200066h.
[31] A. Mannodi-kanakkithodi, A. Chandrasekaran, C. Kim, T.D. Huan, G. Pilania, V. Botu, R. Ramprasad, Scoping the polymer genome : a roadmap for rational polymer dielectrics design and beyond, Mater. Today xxx (2017), https://doi.org/10.1016/j.mattod.2017.11.021.
[32] P. Pankajakshan, S. Sanyal, O.E. De Noord, I. Bhattacharya, A. Bhattacharyya, U. Waghmare, Machine learning and statistical analysis for materials science: stability and transferability of fingerprint descriptors and chemical insights, Chem. Mater. 29 (2017) 4190–4201, https://doi.org/10.1021/acs.chemmater.6b04229.
[33] H. Zhao, X. Li, Y. Zhang, L.S. Schadler, W. Chen, L.C. Brinson, Perspective: NanoMine: a material genome approach for polymer nanocomposites analysis and design, Apl. Mater. 4 (2016), 053204, https://doi.org/10.1063/1.4943679.
[34] M.A. Webb, N.E. Jackson, P.S. Gil, J.J. de Pablo, Targeted sequence design within the coarse-grained polymer genome, Sci. Adv. 6 (2020), https://doi.org/10.1126/sciadv.abc6216 eabc6216.
[35] S. Plimpton, Fast parallel algorithms for short-range molecular dynamics, J. Comput. Phys. 117 (1995) 1–19, https://doi.org/10.1006/jcph.1995.1039.
[36] L.S. Dodda, I.C. De Vaca, J. Tirado-Rives, W.L. Jorgensen, LigParGen web server: an automatic OPLS-AA parameter generator for organic ligands, Nucleic Acids Res. 45 (2017) W331–W336, https://doi.org/10.1093/nar/gkx312.
[37] LAMMPS molecular dynamics simulator (n.d.), http://lammps.sandia.gov.
[38] W.L. Jorgensen, J. Tirado-Rives, The OPLS [optimized potentials for liquid simulations] potential functions for proteins, energy minimizations for crystals of cyclic peptides and crambin, J. Am. Chem. Soc. 110 (1988) 1657–1666, https://doi.org/10.1021/ja00214a001.
[39] W.L. Jorgensen, J.D. Madura, C.J. Swenson, Optimized intermolecular potential functions for liquid hydrocarbons, J. Am. Chem. Soc. 106 (1984) 6638–6646, https://doi.org/10.1021/ja00334a030.
[40] W.L. Jorgensen, D.S. Maxwell, J. Tirado-Rives, N. Haven, Development and testing of the OPLS all-atom force field on conformational energetics and properties of organic liquids, J. Am. Chem. Soc. 118 (1996) 11225–11236, https://doi.org/10.1021/ja9621760.

[41] S. Nosé, A unified formulation of the constant temperature molecular dynamics methods, J. Chem. Phys. 81 (1984) 511–519, https://doi.org/10.1063/1.447334.
[42] C. Li, A. Strachan, Molecular scale simulations on thermoset polymers: a review, J. Polym. Sci., Part B: Polym. Phys. 53 (2015) 103–122, https://doi.org/10.1002/polb.23489.
[43] Y. Fu, J.G. Michopoulos, J.-H.H. Song, On investigating the thermomechanical properties of cross-linked epoxy via molecular dynamics analysis, Nanoscale Microscale Thermophys. Eng. 21 (2017) 8–25, https://doi.org/10.1080/15567265.2016.1263696.
[44] J. Fan, G. Li, High enthalpy storage thermoset network with giant stress and energy output in rubbery state, Nat. Commun. 9 (2018) 642, https://doi.org/10.1038/s41467-018-03094-2.
[45] A. Lendlein, S. Kelch, Shape-memory polymers, Angew. Chem. Int. Ed. 41 (2002) 2034–2057, https://doi.org/10.1002/1521-3773(20020617)41:12<2034:AID-ANIE2034>3.0.CO;2-M.
[46] R. Stepto, T. Chang, P. Kratochvíl, M. Hess, K. Horie, T. Sato, J. Vohlídal, Definitions of terms relating to individual macromolecules, macromolecular assemblies, polymer solutions, and amorphous bulk polymers (IUPAC Recommendations 2014), Pure Appl. Chem. 87 (2015) 71–120, https://doi.org/10.1515/pac-2013-0201.
[49] X. Feng, G. Li, High-temperature shape memory photopolymer with intrinsic flame retardancy and record-high recovery stress, Applied Materials Today 23 (2021) 101056, https://doi.org/10.1016/j.apmt.2021.101056.
[50] C. Yan, G. Li, A mechanism based four-chain constitutive model for enthalpy driven thermoset shape memory polymers with finite deformation, Journal of Applied Mechanics-Transactions of ASME 87 (2020), 061007, https://doi.org/10.1115/1.4046583.